Simulations of Anisotropic Grain Growth: Efficient Algorithms and Misorientation Distributions

Matt Elsey Selim Esedoḡlu Peter Smereka

October 29, 2012

Abstract

An accurate and efficient algorithm, closely related to the level set method, is presented for the simulation of Mullins' model of grain growth with arbitrarily prescribed surface energies. The implicit representation of interfaces allows for seamless transitions through topological changes. Well-resolved large-scale simulations are presented, beginning with over 650,000 grains in two dimensions and 64,000 grains in three dimensions. The evolution of the misorientation distribution function (MDF) is computed, starting from random and fiber crystallographic textures with Read–Shockley surface energies. Prior work had established that with random texture the MDF shows little change as the grain network coarsened whereas with fiber texture the MDF concentrates near zero misorientation. The lack of concentration about zero of the MDF in the random texture case has not been satisfactorily explained previously since this concentration would decrease the energy of the system. In this study, very large-scale simulations confirm these previous studies. However, computations with a larger cutoff for the Read–Shockley energies and an affine surface energy show a greater tendency for the MDF to concentrate near small misorientations. This suggests that the reason the previous studies had observed little change in the MDF is kinetic in nature. In addition, patterns of similarly oriented grains are observed to form as the MDF concentrates.

1 Introduction

Macroscopic properties of a polycrystalline material depend on its crystallographic texture and grain boundary character. These properties can evolve under thermomechanical processing such as heat treatment or deformation. Ignoring recrystallization, the evolution of the texture and the grain boundary character is largely determined by properties of the initial grain boundary network. The motion of this network of surfaces is often modeled as steepest descent for a weighted surface energy, where low angle grain boundaries (formed between adjacent grains with similar orientations and said to have low *misorientation*) receive lower weights than high angle ones. A specific functional dependence due to Read and Shockley [22] with a standard extension for high-angle grain boundaries (see e.g. [12]) is commonly used to assign the weight to a grain boundary in terms of the orientations of the two adjacent grains.

In the anisotropic case there are two aspects to this energy minimization process. First is grain growth: As some grains grow others must shrink, and as such the total length of the grain boundaries must decrease. In fact, in the isotropic case this is the only mode of energy reduction. However, in the anisotropic case, the energy will decrease if the grain boundary energy is reduced. This can happen when two grains with similar orientations happen to meet. Therefore, it might be expected that the distribution of misorientations in the system will also change as the grain network coarsens.

For this reason, a useful statistical descriptor of the grain boundary character is the *misorientation distribution function* (MDF), which measures the relative area of interfaces in the network with a given misorientation. It is useful to note that if the grain boundary energy is isotropic then as the grain network evolves the MDF is expected to remain stationary. On the other hand, if the grain boundary energy is a increasing function of misorientation (as it is often modeled) then one would expect that as the grain network evolves, low misorientation grain boundaries would predominate and as a consequence the MDF would concentrate near small misorientations.

The time evolution of the MDF has attracted attention. Holm et al. [12, 13] studied

the evolution of the MDF via kinetic Monte Carlo (KMC) simulations of grain growth in two dimensions. In one case, orientations were chosen randomly from $SO(3)$, and misorientations were computed with regard to cubic symmetry, resulting in an initial MDF following the well-known Mackenzie distribution [16]. They observed that the MDF evolved into a steady state quite close to the initial Mackenzie distribution, characterized by a slight enhancement of the low misorientation boundaries. More recently, Gruber et al. [9] carried out larger KMC simulations, both in two and three dimensions, that helped remove the statistical uncertainties in some of the results of [12, 13]. Their initial conditions contained over 75,000 well-resolved grains in two dimensions and they obtained essentially the same results as found by Holm et al. [12].

These results are rather surprising in view of the discussion above. From an energetic point of view, one would expect that MDF would concentrate for small misorientations. Indeed, both Holm et al. and Gruber et al. also considered simulations with initial conditions dominated by a single-component texture. In this case they observed that the MDF evolves in such a way that it tends to concentrate at low misorientations. In addition, the fiber texture case was studied by Holm et al. and Kinderlehrer et al. [15] (using front tracking, with a different misorientation to surface energy map). Both investigations observed the concentration of the MDF at zero misorientation.

Barmak et al. [2] went on to further suggest that the MDF converges to a Boltzmann distribution, namely

$$g(\phi) = \frac{1}{Z_\lambda} e^{-\frac{1}{\lambda}\sigma(\phi)} \tag{1}$$

where ϕ is the misorientation, $\sigma(\phi)$ is the grain boundary energy associated with a misorientation ϕ, and Z_λ a normalization factor. Notice if the surface energy is a strictly increasing function of the misorientation angle then (1) will have a maximum value at zero misorientation. From a thermodynamic point of view (1) is reasonable. In addition, there is a remarkable formulation to determine the "thermal energy," λ. This value of λ is the one that yields the fastest decrease of the relative entropy [2]. The difference between the results observed in the fiber texture and strongly textured simulations as compared to the random texture case is remarkable: In the former, concentration of the MDF about zero misorientation is clearly observed. In the latter,

only a small deviation from the Mackenzie distribution is observed. The "stability" of the Mackenzie distribution is peculiar since an energetic point of view suggests that the MDF should tend to concentrate near zero.

We propose to explore this issue with a numerical approach capable of simulating a very large number of grains over much longer periods of time. This is accomplished by introducing a new computational approach to *anisotropic* (unequal surface energy) grain growth that in two dimensions can readily simulate the coarsening of approximately 670,000 grains down to less than 4,000. This new algorithm allows arbitrary surface energies to be specified between any two grains in the network. It is accurate, robust, efficient, and easily parallelized. It builds on the distance function-based diffusion-generated motion (DFDGM) approach [7], which was used in earlier work [4, 5] to simulate long time *isotropic* (equal surface energy) grain growth with very large numbers of grains. The initial simulations presented demonstrate this method recovers previous results using KMC simulations [9, 12, 13] and front tracking [15, 2]. Subsequent simulations demonstrate the importance of the surface energy-to-misorientation map in predicting the time evolution of the MDF and suggests a framework capable of explaining the different MDFs obtained in the fiber texture and random texture cases.

2 The Model

We will use Mullins' model [11, 20] of normal grain growth. Denoting the boundary between two adjacent grains Σ_j and Σ_k as Γ_{jk}, the specific form of Mullins' model we consider is

$$E = \sum_{j<k} \sigma_{jk} \mathrm{Area}\big(\Gamma_{jk}\big). \tag{2}$$

The constants σ_{jk} are known as *surface energies* associated with the Γ_{jk}. In particular, this model ignores the dependence of the energy density on the boundary plane. Moreover, we assume constant mobilities for all Γ_{jk}. Accordingly, Γ_{jk} moves by the normal speed

$$v_n(\Gamma_{jk}) = \sigma_{jk}\, \kappa_{jk}, \tag{3}$$

where κ_{jk} denotes the mean curvature of Γ_{jk}. At a triple junction formed by the meeting of three distinct phases Σ_j, Σ_k, and Σ_ℓ, Herring angle conditions [10] hold; they stipulate:

$$0 = \sigma_{jk} n_{jk} + \sigma_{k\ell} n_{k\ell} + \sigma_{\ell j} n_{\ell j}, \tag{4}$$

so that the angles formed by the normals n_{jk}, $n_{k\ell}$, $n_{\ell j}$ to the three interfaces Γ_{jk}, $\Gamma_{k\ell}$, $\Gamma_{\ell j}$ along the triple curve are determined by the surface energies σ_{jk}, $\sigma_{k\ell}$, and $\sigma_{\ell j}$.

The surface energies σ_{jk} will be assumed to be positive and to respect the triangle inequality

$$\sigma_{jk} + \sigma_{k\ell} > \sigma_{\ell j} \text{ for any distinct } j, k, \text{ and } \ell, \tag{5}$$

which turns out to be necessary to rule out wetting. Otherwise, the σ_{jk} are arbitrary.

3 The Algorithm

This section presents our new algorithm for model (3) and (4) with arbitrarily prescribed surface energies σ_{jk}, suitable for large-scale simulations of grain networks. Our previous work [4, 5] developed an efficient algorithm for the same model in the equal surface energy (i.e. $\sigma_{jk} = 1$) case, in both two and three dimensions. As in that previous work, our approach uses distance function-based diffusion generated motion [7]. The extension described here to arbitrary surface energies from [4, 5] is highly non-trivial. We start by reviewing distance function based diffusion generated motion in its most elementary form.

3.1 Distance Function Diffusion Generated Motion

We start with the simplest setting of two-phase curvature flow: Consider a single grain, Σ, surrounded by another grain of infinite extent. To evolve the boundary $\partial\Sigma$ with normal speed $v_n = \kappa$ using the level set method, one would first take a level set function ϕ so that $\Sigma = \{x : \phi(x) > 0\}$ and $\phi = 0$ on $\partial\Sigma$; then, one would evolve ϕ by $\partial_t \phi = \kappa |\nabla \phi|$. Among the many possible level set representations of Σ, if ϕ is chosen to be the *signed distance function*, d, then the level set equation greatly simplifies:

$\Delta d = \kappa$ along the interface, and $|\nabla d| = 1$, by which the level set equation reduces to $\partial_t \phi = \Delta \phi$. However, during this evolution ϕ will not remain a signed distance function even if it starts as one; it must be reinitialized to remain as such. Therefore, alternating repeatedly these two operations, namely linear diffusion and reinitialization, yields motion by mean curvature. The threshold dynamics scheme proposed in [18, 19] and developed further in [23] for this problem applies a similar approach using the characteristic function of Σ rather than the signed distance function.

To be more precise, let $d^s(x)$ be the signed distance function at times $s\Delta t$, $s = 0, 1, 2, ...$, where Δt is the time step. The solution of the heat equation for one time step with d^s as an initial condition is $G_{\Delta t} * d^s$ where $G_t = (4\pi t)^{-D/2} e^{-|x|^2/(4t)}$ in D dimensions. Finally, $d = \text{Redist}(\phi)$ is the operation that will produce a distance function from ϕ where both d and ϕ have the same zero level set. The resulting algorithm is

Algorithm 1

1. $A = G_{\Delta t} * d^s$
2. $d^{s+1} = \text{Redist}(A)$

Under the algorithm above, the surfaces defined implicitly via $\{d^s = 0\}$ move by an approximation to motion by mean curvature with mobility equal to one; convergence to the exact flow takes place as $\Delta t \to 0$.

In the multiphase setting, let Γ_{jk} denote the boundary between grains Σ_j and Σ_k, with $j, k \in \{1, 2, \ldots, N\}$. Let d_j^s denoted the signed distance function for the j-th grain at time step s; i.e. $\Sigma_j^s = \{x : d_j^s(x) > 0\}$. First, diffuse all of the distance functions d_j^s, denoting the result $A_j^s = G_{\Delta t} * d_j^s$. Then, each spatial point x must be reassigned to a single grain, which is done according to the following rule: If $A_k^s(x)$ is the largest among all the convolutions, then x is assigned to grain k. Thus, the algorithm is:

Algorithm 2

1. $A_j = G_{\Delta t} * d_j^s$
2. $B_j = \frac{1}{2}\left(A_j - \max_{k \neq j} A_k\right)$
3. $d_j^{s+1} = \text{Redist}(B_j)$

The resulting normal speed for the boundary of each grain under Algorithm 2 is $v_n = \kappa$. Furthermore, the relevant Herring angle condition is satisfied along triple curves. Algorithms 1 and 2 are due to Esedoglu et al. [7].

In [4, 5], Algorithm 2 was extended by recognizing that a separate signed distance function is not needed for each individual grain: Well-separated grains can be lumped into families. A single signed distance function is then computed to represent an entire family, which can contain thousands of distant grains. This partitioning is constantly updated to ensure the well-separation of grains belonging to the same family, preventing unphysical interactions and mergers. In practice, as few as 18 families can be sufficient to simulate over $670,000$ grains in two dimensions. This procedure will be discussed in more detail below. In [6], we further extended this algorithm to models of recrystallization. The schemes have thus proven their mettle in very large-scale, fully resolved, accurate simulations in both two and three dimensions, handling hundreds of thousands of topological changes along the way.

3.2 Arbitrary Surface Energies

Extending DFDGM to the case of arbitrarily prescribed surface energies, the algorithmic meat of the present paper, is based on two observations. First, Algorithm 2 for equal surface energies extends to the *additive* surface energy case quite easily. We call a set of surface energies σ_{jk} additive if they arise as

$$\sigma_{jk} = \frac{1}{2}(\gamma_j + \gamma_k), \tag{6}$$

for N arbitrarily chosen nonnegative weights γ_j. Note that this is a very small subset (of dimension N) of all admissible surface energies (a set of dimension $N(N-1)/2$). Nevertheless, our second observation is that *any* three-grain model satisfying (3) and (5) can be expressed in terms of the additive case. The energy (2) of the system becomes

$$E = \sum_{j=1}^{N} \gamma_j \mathrm{Area}(\partial\Sigma_j). \tag{7}$$

This suggests the following modification to Algorithm 2:

Algorithm 3

1. $A_j = G_{\gamma_j \Delta t} * d_j^s$
2. $B_j = \frac{1}{2}\left(A_j - \max_{k \neq j} A_k\right)$
3. $d_j^{s+1} = \text{Redist}(B_j)$

Notice that the only difference between Algorithms 2 and 3 is the convolution kernel used in the first step. Under Algorithm 3, the normal speed of the grain boundary Γ_{jk} is $v_n = \frac{1}{2}(\gamma_j + \gamma_k)\kappa$. Numerical tests presented in Section 3.3 indicate that the appropriate Herring angle conditions (4) are also enforced by this modified algorithm.

One drawback of Algorithm 3 compared to Algorithm 2 is the necessity to represent and convolve each grain separately. In our original Algorithm 2, all grains are convolved with the same Gaussian kernel, allowing us to represent many well-separated grains with a single signed distance function to their union, which allows computing their convolutions all at once. This allowed for great computational efficiency and the simulation of over one hundred thousand well-resolved grains in both two and three spatial dimensions. In Algorithm 3, as each grain may be associated with a different value of γ_j, either the convolutions must be performed locally (prohibiting the use of the efficient discrete Fourier transform), or each grain must be represented in its own signed distance function. To redress this drawback of Algorithm 3, we make the following observation:

Let Ξ_j denote the union of all grains represented by d_j, i.e. $\{d_j > 0\} = \Xi_j$. Next, we define $\gamma_j(x) = \gamma_k$ for the grain $\Sigma_k \subseteq \Xi_j$ nearest to x. We can now replace A_j in the Algorithm 3 by

$$A_j(x) = \frac{\gamma_j(x)}{\gamma^*}\left(G_{\gamma^* \Delta t} * d_j^s\right) + \left(1 - \frac{\gamma_j(x)}{\gamma^*}\right) d_j^s, \tag{8}$$

with $\gamma^* = \max_i \gamma_i$. It can be shown that the expressions for A_j given above and in step 1 of Algorithm 3 agree to $O(\Delta t)$ along smooth interfaces Γ_{ij} away from triple junctions.

Let Algorithm 4 denote the modification of Algorithm 3 that replaces its step 1 with (8). The major resultant gain is the use of a single convolution kernel, which allows computing the convolutions of many grains all at once with a single FFT and

inverse FFT pair.

Next, observe that in the three-phase case, arbitrary surface energies σ_{12}, σ_{13}, and σ_{23} can be mapped to γ_1, γ_2, γ_3 so that $\sigma_{12} = (\gamma_1 + \gamma_2)/2$, etc., by the mapping

$$\begin{pmatrix} \gamma_1 \\ \gamma_2 \\ \gamma_3 \end{pmatrix} = \begin{pmatrix} 1 & 1 & -1 \\ 1 & -1 & 1 \\ -1 & 1 & 1 \end{pmatrix} \begin{pmatrix} \sigma_{12} \\ \sigma_{13} \\ \sigma_{23} \end{pmatrix} \tag{9}$$

where the triangle inequality for σ_{jk} implies that γ_j are positive. This observation has independently been made recently by [17]. Thus, Algorithm 3 is sufficient to generate three-phase motion with arbitrarily chosen surface energies. For N-phase motion, we note that there is, in general, no assignment of surface energies γ_j so that the arbitrary σ_{jk} can be written as $\sigma_{jk} = (\gamma_j + \gamma_k)/2$.

Algorithm 3 or 4, together with (9), can be used to update grain boundaries Γ_{jk}, including at and around triple curves. Note that quadruple junctions are common at all times on the face of three-dimensional grains as the meeting place of triple curves, and higher multiplicity junctions arise, e.g. during topological transitions. We now explain how four and higher multiplicity junctions are handled.

Our approach is related to the weighted averages used in [23] for handling junctions of high multiplicity. In our version, for a phase j present at the junction, we calculate convolution values for each of the triple junctions it can form with any two of the remaining phases at the same junction, and take a weighted average of how it would have been updated had it been at a triple junction with them. Consider the case of a quadruple junction. First, compute A_j as given in (8) for the γ_j computed by (9) for each of the three possible triplets that phase j can participate in, and denote those values $\psi_{j;k\ell}$. For example, for $j = 1$ we apply (9) and (8) to compute $\psi_{1;23}$, $\psi_{1;34}$, and $\psi_{1;24}$. Next we compute the quantity

$$T_1(x) = \frac{1}{3}\left(\psi_{1;23} + \psi_{1;34} + \psi_{1;24}\right)$$

Analogous quantities T_2, T_3 and T_4 are also computed.

An important observation is that

$$\text{if } x \text{ is well inside of } \Sigma_j \text{ then } A_j(x) > K \text{ and}$$

$$\text{if } x \text{ is well outside of } \Sigma_j \text{ then } A_j(x) < -K,$$

where $K = 2.5\sqrt{\Delta t \log(1/(4\pi\Delta t))}$. By "well inside (outside)," we mean that a single step of Algorithm 4 will not bring x out of (into) set Σ_j. It therefore follows that if x is well inside grain Σ_1 then $T_1(x) > K$ and if x is well outside grain Σ_1 then $T_1(x) < -K$. This leads us to define the following weight function

$$w_j(x) = \begin{cases} \varepsilon, & T_j(x) < -K \\ \varepsilon + (1-\varepsilon)\left(\frac{1}{2} + \frac{T_j(x)}{2K}\right), & |T_j(x)| < K \\ 1, & T_j(x) > K. \end{cases} \tag{10}$$

Therefore if $w_1(x) = 1$ then we are in grain Σ_1 and if $w_1(x) = \varepsilon$ we are not in grain Σ_1. $w_2(x)$, $w_3(x)$, and $w_4(x)$ are also computed.

To understand the third step, consider the quantity $w_1 w_j w_k$ and let the values j_M and k_M be the j and k, respectively, that maximize it. Then grains j_M and k_M are interacting most strongly with grain Σ_1. This would suggest that we might replace A_1 by $\psi_{1;j_M,k_M}$. In practice, we do something smoother, namely

$$A_1(x) = \frac{\sum_{j,k=2,\, j<k}^{4} w_1 w_j w_k \, \psi_{1;jk}}{\sum_{j,k=2,\, j<k}^{4} w_1 w_j w_k}.$$

In a similar way we compute A_2, A_3, A_4. The above procedure now replaces step 1 of Algorithms 3 or 4.

The general algorithm is now stated.

Algorithm 5: Full Algorithm for Arbitrary Surface Energies

Fix Δt, ε and $K > 0$. Define $\gamma_{j;k\ell}$ to be the weight γ_j obtained from solving (9) with inputs σ_{jk}, $\sigma_{k\ell}$, and $\sigma_{\ell j}$, and $\psi(x, d_j^s, \sigma_j(x))$ to be the right-hand side of (8). Define $M \le N$ collections Ξ_j of disjoint grains so that $\bigcup_{j=1}^{M} \Xi_j = \bigcup_{j=1}^{N} \Sigma_j$. Maintain M signed distance functions $d_j(x)$, giving the signed distance to the collection Ξ_j, with $d_j(x) > 0$ for $x \in \Xi_j$. The signed distance functions are updated by the following:
For $s = 0, \ldots, s_{\max}$ and $j = 1, \ldots, M$, perform steps 1–4.

1. UPDATE: For each grid location x, define $R(x) = \{i : d_i(x) > -\varepsilon\}$, and let $r(x) = \#R(x)$.

   (a) If $R(x) = \{j\}$, set $A_j(x) = d_j^s(x)$.

   (b) If $R(x) = \{j, k\}$, set $A_j(x) = \psi(x; d_j^s, \sigma_{jk})$, and $A_k(x) = \psi(x; d_k^s, \sigma_{jk})$.

   (c) If $R(x) = \{j, k, \ell\}$, set $A_j(x) = \psi(x; d_j^s, \gamma_{j;k\ell})$, $A_k(x) = \psi(x; d_k^s, \gamma_{k;j\ell})$, and $A_\ell(x) = \psi(x; d_\ell^s, \gamma_{\ell;jk})$.

   (d) If $r(x) > 3$,

   - For each $i \in R$, compute

$$T_i(x) = \frac{1}{\binom{r(x)-1}{2}} \sum_{\substack{j,k \in R\setminus\{i\} \\ j<k}} \psi(x; d_i^s, \gamma_{i;jk}). \tag{11}$$

   - Next compute $w_i(x)$ by (10).

   - Set

$$A_i(x) = \frac{\displaystyle\sum_{\substack{j,k \in R\setminus\{i\} \\ j<k}} w_i w_j w_k \, \psi(x; d_i, \gamma_{i;jk})}{\displaystyle\sum_{\substack{j,k \in R\setminus\{i\} \\ j<k}} w_i w_j w_k}. \tag{12}$$

2. REDISTRIBUTE: Construct

$$B_j(x) = \frac{1}{2}\left(A_j(x) - \max_{k \neq j} A_k(x)\right) \tag{13}$$

   to remove overlaps and vacuums from the previous step.

3. REDISTANCE: Set $C_j(x)$ to be the signed distance function to the zero-level set of $B_j(x)$.

4. SWAP: As necessary, swap appropriate grains between signed distance functions C_j to ensure a minimum separation between grains associated with the same signed distance function. Redistance around swapped grains and denote the resulting signed distance functions as $d_j^{s+1}(x)$.

3.3 Validation

In this section we provide numerical results demonstrating the accuracy of Algorithms 3, 4, and 5. The first two examples are three-phase evolutions: A generalized version

of the well-known "Grim Reaper" exact solution, and an initial conditions devoid of symmetry where we compare with front tracking. Then, we investigate the ability of Algorithm 5 to preserve stable quadruple junctions, the existence of and conditions for which have been previously studied by Cahn [3].

3.3.1 "Grim Reaper" Profile

A derivation for a constantly transported profile in the axially symmetric case $\sigma_{12} = \sigma_{13}$, commonly referred to as the "Grim Reaper," is given in the Appendix of [8]. We straightforwardly extend this calculation to the more general case where all surface energies may be chosen independently of each other. The derivation is omitted but follows that in [8] closely. We choose $\sigma_{12} = 1$, $\sigma_{13} = 0.8$, and $\sigma_{23} = 1.2$. The simulation was performed using Algorithms 3, 4, and 5. All results are in good qualitative agreement. We measure the interfacial velocity by interpolating to find the location of the interfaces corresponding to $\mu_{12}(x)$ and $\mu_{13}(x)$ at $t = 0$ and $t = 3/128$. The L^2 error in interfacial velocity converges approximately linearly. The maximal error occurs near the triple junctions and appears to be converging at a sublinear rate. These results agree with analysis performed on the basic, isotropic algorithm in [7].

3.3.2 Comparison to Front Tracking

To verify that the numerics of the previous experiment are not influenced by the axial symmetry or the vertical interface of the "Grim Reaper" profile, we also study a three-phase evolution with asymmetric curved interfaces. In this case, an exact solution is not known, so we compare with a very high resolution front-tracking simulation containing over $4,800$ points instead. The results obtained are displayed in Figure 1(a). The evolving front-tracking solution was periodically reparameterized to maintain approximately constant spacing between the discretized points. The surface energies were chosen as $\sigma_{12} = 1$, $\sigma_{13} = 2/3$, and $\sigma_{23} = 4/3$; here, the first phase is the upper interior region, the second phase is the "background," and the third phase is the lower interior region. The numerical solutions generated by Algorithms 3, 4, and 5 were compared to the reference solution generated by the front tracking code. Due

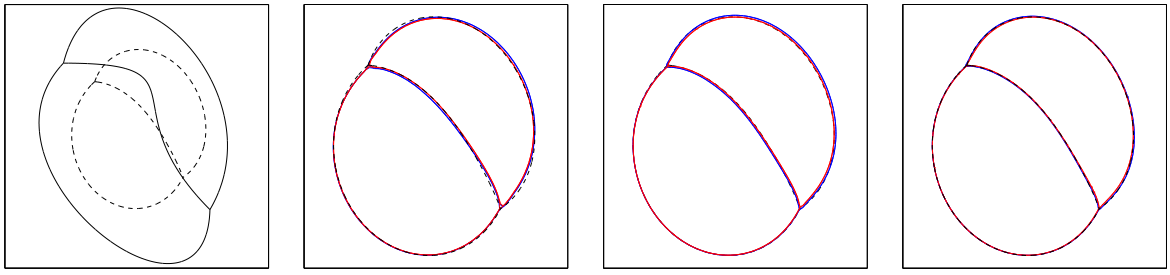

(a) (b) (c) (d)

Figure 1: (a) The initial condition (solid line) and final result (dashed line) obtained by the front tracking code for the simulation of Section 3.3.2. The results obtained by the algorithm proposed here Algorithm 4 (red) and Algorithm 5 (blue) are displayed in (b), (c), and (d), with $\Delta x = 1/128$, $1/256$, and $1/512$, respectively. They are visually indistinguishable from the front tracking solution (dashed line) for resolutions $\Delta x \leq 1/512$ at this scale.

to very close agreement between Algorithms 3 and 4, only the results obtained from Algorithms 4 and 5 are displayed in Figure 1. Due to the excellent agreement between the various algorithms, we use Algorithm 5, which allows for the full generality of (3), in all subsequent simulations.

3.3.3 Stable Quadruple Junctions

With equal surface energies, quadruple junctions are unstable under multiphase curvature motion in the plane. Cahn [3] investigated the stability of quadruple junctions in the case where there are two "types" of phases, which he denotes type α and type β. Let $q_{\alpha\beta\gamma\delta}$ describe a quadruple junction with the α and γ phases opposite each other. The condition

$$\sigma_{\alpha\alpha}^2 + \sigma_{\beta\beta}^2 \geq 4\sigma_{\alpha\beta}^2 \tag{14}$$

is shown to be necessary and sufficient condition for a $q_{\alpha\beta\alpha\beta}$ quadruple junction to be stable over a range of opening angles. Denote the opening angle of the α phases to be Φ_α and the opening angle of the β phases to be Φ_β. As long as Φ_α is larger than the angle θ_α arising from the Herring angle condition (4) for the $t_{\alpha\beta\beta}$ triple junction and Φ_β is larger than the angle θ_β for the $t_{\beta\alpha\alpha}$ triple junction, the quadruple junction remains stable.

In our tests, we considers phases Σ_1 and Σ_3 to be of type α (see Figure 2), and

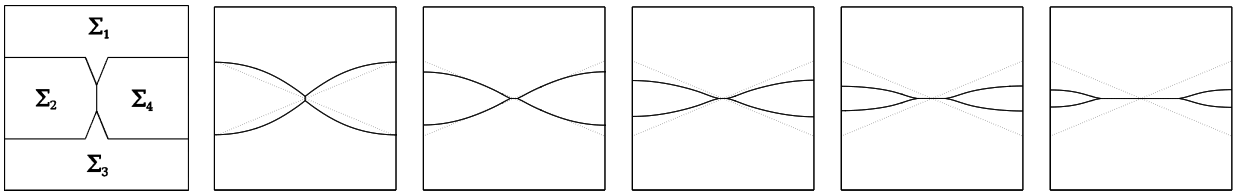

Figure 2: Evolution proceeds from left to right, top to bottom. Surface energies are chosen so that the quadruple junction is stable until the angles made by phases Σ_2 and Σ_4 at the quadruple junction are smaller than those indicated by the dashed guide lines. Good agreement is seen with this analytical prediction.

phases Σ_2 and Σ_4 to be of type β. In the first simulation, we choose $\sigma_{\alpha\alpha} = \sigma_{\beta\beta} = 1.85$, and $\sigma_{\alpha\beta} = 1$. The $q_{\alpha\beta\alpha\beta}$ junction should be stable as long as both Φ_α and Φ_β are greater than $\arccos(.71125) \approx 44.66°$. $\Phi_\beta = \arccos(.71125)$ is marked in dashed lines on Figure 2. Numerically, the quadruple junction does persist (appearing as two triple junctions separated by a Γ_{13} interface which has length $O(\Delta x)$) until Φ_β passes through the critical angle.

4 Large-Scale Simulations

In this section, we use Algorithm 5 to study the evolution of large networks of grains starting from random and fiber textured initial data, as discussed in the introduction. Simulations are performed in both two and three spatial dimensions. Computational requirements allow for the two-dimensional simulations to be initialized with over 650,000 well-resolved grains. In three dimensions, we take an initial condition with approximately 64,000 well-resolved grains. We focus primarily on the results from the simulations performed in two spatial dimensions, as the results are more statistically reliable due to the larger number of grains; however, qualitatively similar results are observed in three spatial dimensions. The results seen in these simulations will be seen to confirm the observations of the prior numerical work [1, 2, 9, 12, 13].

4.1 Two Spatial Dimensions

As discussed in the introduction, two significantly differing types of simulation results have been seen in the literature. For randomly textured initial conditions, KMC simu-

lations [9, 12, 13] show only slight evolution from the initial MDF, which is a Mackenzie distribution. In contrast, the strong single component texture and fiber textured simulations [12, 13, 15] demonstrate sharpening of the MDF about zero misorientation from an initially uniform MDF. We perform a number of very large-scale, well-resolved simulations in two spatial dimensions to (1) confirm the results of these other much smaller simulations and (2) to give an explanation for the dissimiliar character of these results.

4.1.1 Effect of Texture

We begin by comparing two simulations with different initial orientation distributions. In the first simulation, fiber-textured grain orientations are assigned, so only the angle in the axis–angle description of grain orientation varies, and are chosen uniformly at random. In the second simulation, fully random orientations from $SO(3)$ are assigned to each grain.

The simulations were initialized with same microstructure of 671,088 well-resolved grains, chosen as the approximate Voronoi diagram to points placed uniformly at random in the simulation domain. The simulations were run until $t = 1.22 \times 10^{-3}$, when less than 4,000 grains remain in each case. To make the computation on this long time scale computationally feasible, the simulation begin on a 8192×8192 grid discretizing $[0, 1)^2$, and is downsampled onto a 2048×2048 grid at $t = 7.15 \times 10^{-5}$, when less than 40,000 grains remain in each simulation. The time step is also commensurately increased at this time.

The surface energy σ_{jk} is determined based on the following mollified Read-Shockley relationship [22]:

$$\sigma_{jk} = \begin{cases} \sigma_{\min} + (1 - \sigma_{\min}) \frac{|\phi_{jk}|}{\phi_{\max}} \left[1 - \log \left(\frac{|\phi_{jk}|}{\phi_{\max}} \right) \right] & \text{if} \quad |\phi_{jk}| \leq \phi_{\max} \\ 1 & \text{if} \quad |\phi_{jk}| > \phi_{\max}. \end{cases} \tag{15}$$

where ϕ_{jk} is the misorientation angle between the j-th and k-th grains. The value $\sigma_{\min}$ is chosen to be 1/10 to prevent numerical artifacts related to stationary interfaces. For these simulations, we choose $\phi_{\max} = 30^\circ$ to agree with simulations performed in [9, 12]

and to lie within the experimentally observed range [24].

The results for the fiber texture case and the random texture case are shown in Figure 3. The evolution of the MDF for each case is shown in Figures 3(b,e). The initial MDF (thin red bars) is approximately uniform in the fiber texture case. The MDF is seen to rapidly sharpen around zero misorientation, consistent with prior investigations [12, 13, 15]. For random texture, the MDF is initially the Mackenzie distribution. Our simulations show that the MDF evolves very slowly in time revealing only a slight preference for low misorientation grain boundaries at the expense of high misorientation grain boundaries. These results are also consistent with the KMC simulations of [9, 12].

Let us now examine the grain microstructure. In the fiber texture case, the crystallographic orientation is determined by a single angle. This means its orientation can be easily represented by a color scale. The entire microstructure is displayed at time $t = 1.15 \times 10^{-3}$ (Figure 3(a)). We observe that grains of similar orientations tend to form connected domains, a phenomena we shall refer to as grain clustering. The interfaces between grains of similar orientations have very small surface energies associated with them, and so have lower velocities and contribute much less to the energy of the system than the interfaces between grains of very different orientations; as such, it is reasonable that these interfaces disappear much more slowly than high-misorientation interfaces. At the end of the simulation, remaining high–energy interfaces (interfaces between grains of very different orientations) tend to be quite straight. Badmos et al. [1] also reported the phenomena of grain clustering, on much a smaller scale, using front tracking.

We point out that the formation of grain clusters should be expected from general considerations. As the grain network coarsens the orientation distribution of the grains is not expected to change. However, it is energetically favorable for grains with similar orientations to be next to each other. Therefore, over time one might expect clusters of grains to form. Since the orientation distribution does not change significantly as the grain network evolves, this clustering phenomena can be rather complex.

For the random texture case, we make use of a coloring scheme designed by Patala

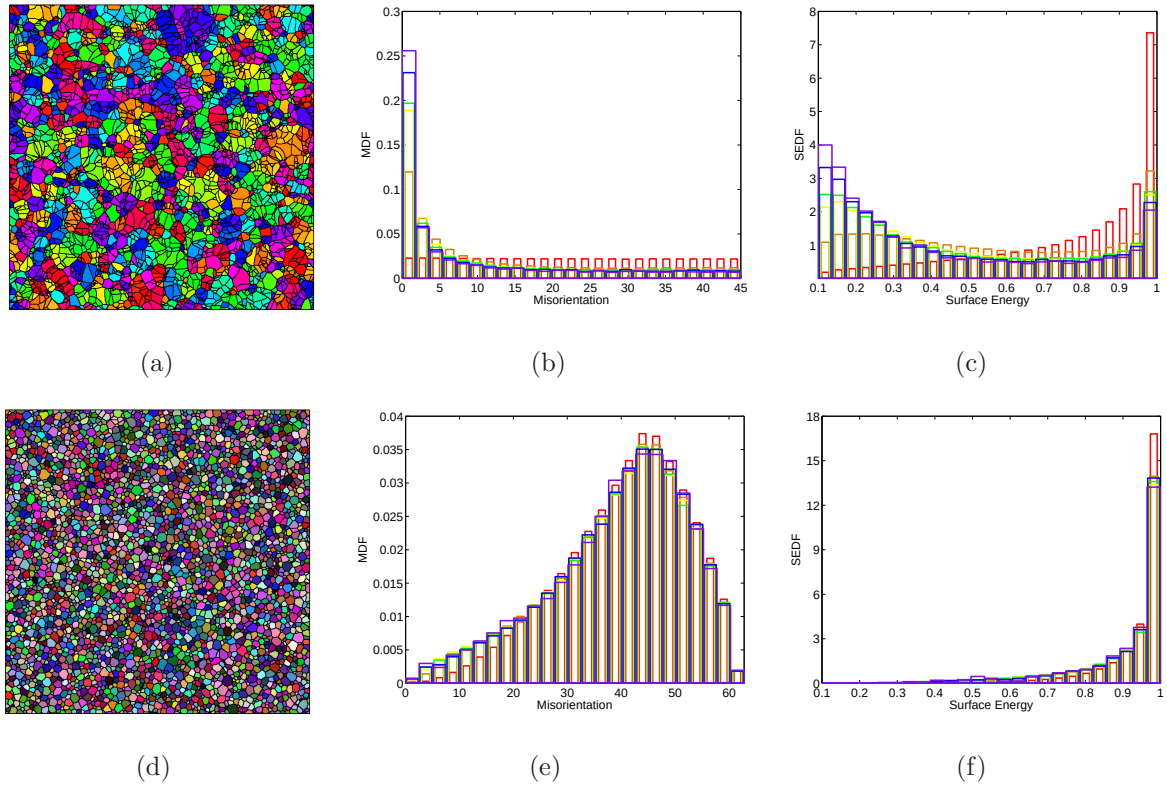

(a) (b) (c)

(d) (e) (f)

Figure 3: Comparison of two-dimensional simulation results. The top row shows results from the fiber texture simulation, while the bottom row shows results from the random orientation case. From left to right: The full microstructure when approximately 4,000 grains remain, and the evolution of the MDF and the SEDF (wider bars correspond to later times). The surface energy is Read–Shockley, with $\phi_{\max} = 30°$. For the fiber texture case, grains are colored by orientation angle so that grains of similar orientations have like colors. Large connected components composed of grains of similar orientations are observed to form. In the random case, grains are colored by misorientation to a randomly-chosen reference grain using the algorithm of Patala, et al. [21]. The spatial grouping of grains of similar orientation is not observed as in the fiber texture case. The MDF concentrates about 0° misorientation in the fiber texture case but remains close to the Mackenzie distribution in the random texture case. The SEDF shows that there are many more low–energy grain boundaries present initially in the fiber texture case than in the random texture case.

et al. [21] which maps the fundamental zone for cubic symmetry (432-misorientation space) onto the HSV color space in such a way that low misorientations are represented by lighter colors and high misorientations are represented by darker colors. Following their work, we select a reference grain randomly among those surviving until the end of the simulation, and color all grains by their misorientation with respect to this particular grain. Snapshots of the microstructure when 4,000 grains remain are shown in Figure 3(d). In contrast to the fiber texture case, there appears to be no significant grain clustering. While consistent with the result that the MDF did not change much

from the initial Mackenzie distribution, it is surprising that clusters seem to be unable to form.

To gain some insight into this, we introduce the distribution of surface energies and define the histogram of area-weighted grain boundaries as a function of surface energy to be the *surface energy distribution function* (SEDF). It is customary in both experiment and simulation to study the MDF rather than the SEDF. From an experimental viewpoint, it is much easier to measure grain orientations than it is to measure surface energies. The former can be measured, for example, by electron backscatter diffraction techniques. In contrast, the latter is indirectly measured using a variety of techniques [14] (for example, by measuring triple junction angles and appealing to (4)). However, no such barrier exists in our numerical simulations. Indeed, a functional form for surface energy as a function of misorientation is assumed and thus the surface energy of any interface can be determined directly from the simulation results.

In the Read–Shockley case, the SEDF is initially very sharply peaked about the maximum surface energy (Figure 3(f)). Very few interfaces interact with any other surface energy, and so there is little opportunity for the system to form low misorientation interfaces. In contrast, fiber texture case has an initial SEDF that is less sharply peaked at the maximum surface energy (Figure 3(c), note the different scale) and has a significant fraction of low energy grain boundaries. As a consequence, more interfaces feel a sub-maximal surface energy, allowing the grain network to more quickly lower its total energy. As the MDF concentrates near zero, grain clustering occurs.

4.1.2 Effect of Surface Energy

In order to more fully explain the differences in results of the fiber texture and random texture simulations presented previously, the role played by the surface energies must be more fully appreciated. To this end, we perform two additional simulations. In these simulations, we take the same randomly-textured initial microstructure as before, but assign different forms of the surface energy. We choose an affine surface energy function,

$$\sigma_{jk} = \sigma_{\min} + (1 - \sigma_{\min}) \frac{|\phi_{jk}|}{\phi_{\max}} \tag{16}$$

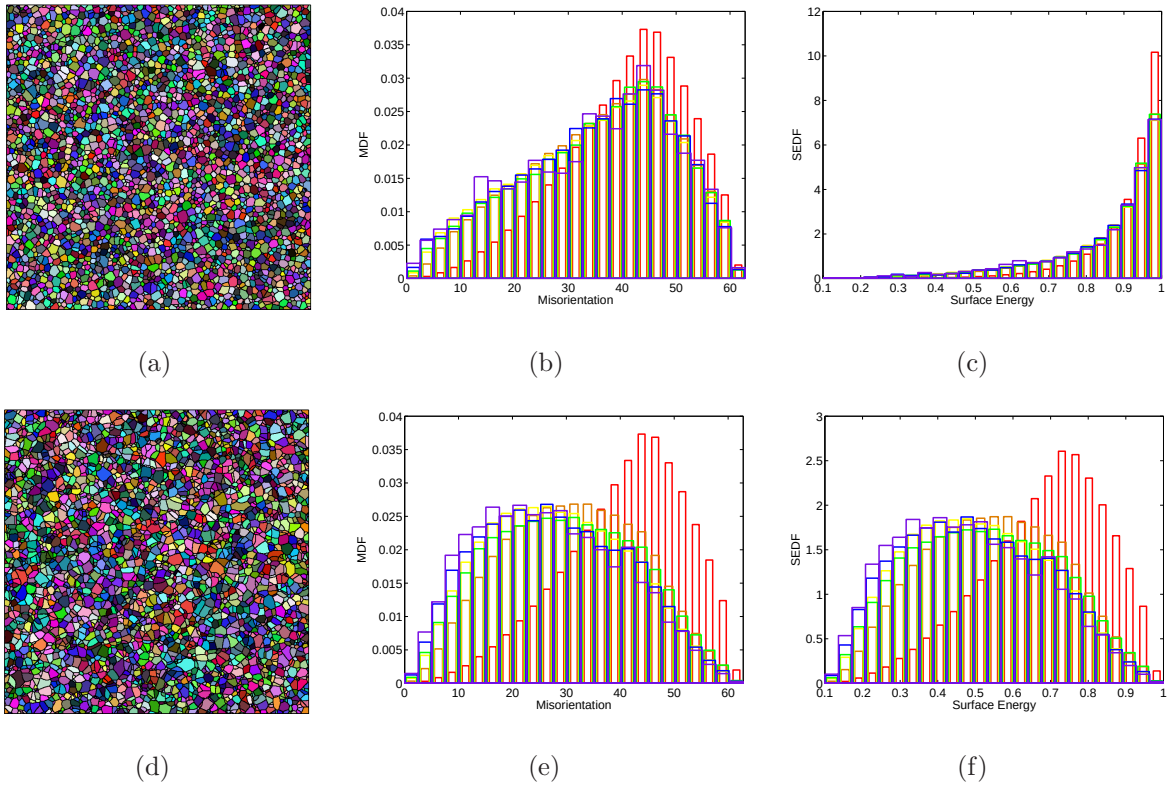

Figure 4: Full microstructure of simulations initialized with random texture when 4,000 grains remain, and time evolution of the MDF and SEDF for the Read–Shockley surface energy (a–c) and the affine surface energy (d–f), both with $\phi_{\max} = 62.8°$. The MDF evolves much more with the affine surface energy, though both MDFs are initially Mackenzie. The SEDF shows that far fewer low–energy grain boundaries are present initially in the Read–Shockley case than in the affine case.

and also again consider the Read–Shockley surface energy. In these cases, we again choose $\sigma_{\min} = 1/10$ but now choose $\phi_{\max}$ to be the maximum possible misorientation, $\approx 62.8°$. These forms both satisfy the triangle inequality (5).

Figure 4 shows the microstructure of these new simulations when 4,000 grains remain, and the time evolution of the MDF and SEDF, with the Read–Shockley surface energy in the top row and the affine surface energy below. Both simulations initially have the Mackenzie distribution as the initial MDF; however, in both cases the time evolution of the MDF is noticeably different from the Read–Shockley case with $\phi_{\max} = 30°$. The difference is most pronounced in the affine case. The differences in each of these three cases can be understood by the corresponding initial SEDFs. If we compare the SEDF for the Read–Shockley case with $\phi_{\max} = 60°$ with the one

for $\phi_{\max} = 30^\circ$ we see that it is less concentrated at the maximum surface energy and comparing with the affine case the SEDF is dramically different — there is no concentration at the highest surface energy.

When the SEDF is heavily concentrated at the highest surface energy, it means very few interfaces feel any other surface energy, and so there is little opportunity for the system to form low misorientation interfaces. In contrast, the affine surface energy gives an initial SEDF which is shaped like the Mackenzie distribution. This means that many more interfaces have a sub-maximal surface energy in this case and are thus energetically preferred to survive. Thus the lower misorientation interfaces are even more preferred, and the MDF evolves to reflect this. This effect can be controlled by the value of $\phi_{\max}$. As $\phi_{\max} \to 0$, the surface energy function becomes uniform and the SEDF is completely concentrated at its maximal value. Since the network is independent of the grain orientations in this case, we expect that the MDF should remain exactly a Mackenzie distribution. Following this logic, we speculate that the reason the MDF stays close to the Mackenzie distribution for nonzero values of $\phi_{\max}$ is that the energy pathway for minimization is kinetically limited.

Finally, we remark that in these two cases we see some evidence of grain clustering but it is certainly not as prominent as in the fiber texture case. This is consistent with the evolution of the MDF. In both of these cases the MDF was only enhanced at low misorientations whereas in the fiber texture case a strong concentration of the MDF at zero misfit was observed. Therefore is reasonable to expect more grain clustering in the fiber texture case as compared to the random texture case.

4.2 Three Spatial Dimensions

In three dimensions, the simulation is performed on a $400 \times 400 \times 400$ grid discretizing $[0, 1)^3$. The initial microstructure contains 64,000 grains. Orientations are assigned uniformly at random. Three simulations are run until $t = 8.50 \times 10^{-3}$. At this time, fewer than 1,050 grains remain in each simulation. The first simulation, with microstructure and MDF shown in Figure 5, takes the Read–Shockley surface energy with $\phi_{\max} = 30^\circ$. The simulation is repeated, as before, with the same initial mi-

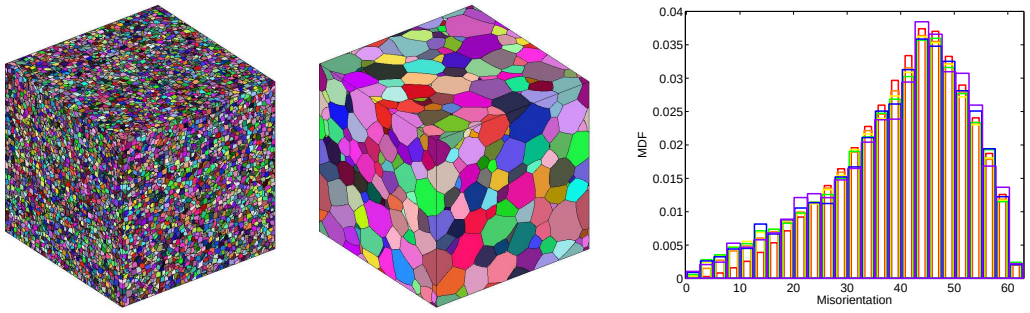

(a) (b) (c)

Figure 5: (a) The initial microstructure contains 64,000 grains. (b) At the end of simulation, only 616 grains remain. (c) The evolution of the MDF through time shows a slight increase at low misorientation.

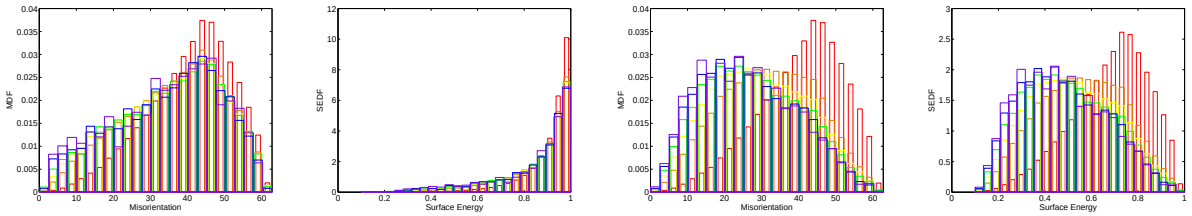

(a) (b) (c) (d)

Figure 6: For fully three-dimensional simulations, time evolution of the MDF (a) and SEDF (c) for Read–Shockley surface energies with $\phi_{\max} = 62.8°$ and the MDF (b) and SEDF (d) for the affine surface energy. Compare to Figure 4(b,c,e,f).

crostructure and orientations, but with the Read–Shockley surface energy and affine surface energy with $\phi_{\max} = 62.8°$. Too few grains remain at the end of the simulation to make statistical inferences about the evolution of the MDF, but the evolution of the MDFs and SEDFs, shown in Figure 6, is in qualitative agreement with the results in two spatial dimensions. In this case, the simulation was not large enough to observe the presence or absence of any grain clustering.

5 Summary

We have introduced an algorithm for simulating multiphase curvature motion with arbitrary surface energies. The algorithm represents interfaces implicitly, and much like a level set method, allows for automatic handling of topological changes. In addition,

this method is unconditionally stable and achieves good accuracy on uniform grids. We have demonstrated that this algorithm is useful for simulations of normal grain growth — an important problem in computational materials science. The algorithm can be extended to include other physical effects, for example, the addition of bulk energy terms for modeling recrystalization can be incorporated using the approach proposed by Elsey et al. [6]. Further generalizations, for example to anisotropic surface energies, are currently under investigation.

The numerical simulations described here show good agreement with the results of prior simulations [9, 12, 13, 15] but allow for the accurate evolution of much larger grain boundary networks. These simulations show that the MDF evolves quite differently in the fiber texture and random texture cases. In particular, the MDF concentrates at zero misorentation for the fiber texture case whereas in the random texture case the MDF remains close to its initial Mackenzie distribution. Our large-scale simulations reveal that different microstructures arise in these two cases. In the fiber texture case, grains of similar orientation cluster together whereas in the random texture case this does not appear to occur. We argue that while clustering would further decrease the energy in the random texture case, the rarity of low-misorientation interfaces makes clustering difficult to achieve by grain growth kinetics.

Our simulations suggest that the difference in the evolution of the grain network between the fiber texture and randomly textured cases is kinetic in nature and is tied to the properties of the initial conditions. In the random texture case many fewer grains have low misorientation as compared to the fiber texture case. For example, with fiber texture crystallography, 22% of interfaces initially can be expected to have misorientation of less than 10°. On the other hand, for the random texture case, less than 0.7% of randomly selected interfaces are expected to have such a low misorientation and over 80% of randomly selected interfaces have misorientations greater than 30°. Using the Read–Shockley surface energy (15) with $\phi_{\max} = 30°$, this means that the vast majority of interfaces will have the maximal surface energy. Such a simulation has only a small proportion of interfaces with lower surface energy and so it must be expected that the evolution of the MDF in this regime will be dramatically slower. Indeed, our simu-

lations using the Read–Shockley surface energy with $\phi_{\max} = 30^\circ$ show little change in the MDF whereas using the Read–Shockley surface energy with $\phi_{\max} = 62.8^\circ$ and the affine surface energy show the MDF evolving quite far from a Mackenzie distribution. We observe similar behavior in three dimensional simulations as well. Finally, we mention that this work seems to suggest that as the MDF concentrates for low misorentations clusters of grains with a similar orientation must occur.

6 Acknowledgments

This work was supported, in part, by grants from the National Science Foundation: DMS-0748333, DMS-0810113, DMS-0854870, DMS-1026317, and DMS-1115252. Matt Elsey was also supported by the Rackham Predoctoral Fellowship and NSF grant OISE-0967140. Selim Esedoḡlu was also supported by an Alfred P. Sloan Foundation fellowship.

References

[1] Badmos, A. Y., Frost, H. J., and Baker, I. Simulation of microstructural evolution during directional annealing with variable boundary energy and mobility. *Acta Mater. 51* (2003), 2755–2764.

[2] Barmak, K., Eggeling, E., Emelianenko, M., Epshteyn, Y., Kinderlehrer, D., Sharp, R., and Ta'asan, S. Critical events, entropy, and the grain boundary character distribution. *Phys. Rev. B 83* (2011), 134117.

[3] Cahn, J. W. Stability, microstructural evolution, grain growth, and coarsening in a two-dimensional two-phase microstructure. *Acta Metallurgica et Materialia 39*, 10 (1991), 2189–2199.

[4] Elsey, M., Esedoḡlu, S., and Smereka, P. Diffusion generated motion for grain growth in two and three dimensions. *J. Comp. Phys. 228*, 21 (2009), 8015–8033.

[5] Elsey, M., Esedoḡlu, S., and Smereka, P. Large scale simulation of normal grain growth via diffusion generated motion. *Proc. R. Soc. Lond. A 467* (2011), 381–401.

[6] Elsey, M., Esedoḡlu, S., and Smereka, P. Large-scale simulations and parameter study for a simple recrystallization model. *Phil. Mag. 91*, 11 (2011), 1607–1642.

[7] Esedoḡlu, S., Ruuth, S., and Tsai, R. Diffusion generated motion using signed distance functions. *J. Comp. Phys. 229*, 4 (2010), 1017–1042.

[8] Garcke, H., Nestler, B., and Stoth, B. A multiphase field concept: Numerical simulations of moving phase boundaries and multiple junctions. *SIAM J. Appl. Math. 60*, 1 (1999), 295–315.

[9] Gruber, J., Miller, H. M., Hoffmann, T. D., Rohrer, G. S., and Rollett, A. D. Misorientation texture development during grain growth. part I: Simulation and experiment. *Acta Mater. 57* (2009), 6102–6112.

[10] Herring, C. Surface tension as a motivation for sintering. In *The Physics of Powder Metallurgy*, W. Kingston, Ed. McGraw–Hill, New York, 1951, pp. 143–179.

[11] Hillert, M. On the theory of normal and abnormal grain growth. *Acta Metall. 13* (1965), 227–238.

[12] Holm, E., Hassold, G., and Miodownik, M. On misorientation distribution evolution during anisotropic grain growth. *Acta Mater. 49* (2001), 2981–2991.

[13] Holm, E. A., Hassold, G. N., and Miodownik, M. A. Dimensional effects on anisotropic grain growth. In *Recrystallization and Grain Growth* (2001), G. Gottstein and D. Molodov, Eds., Springer–Verlag, pp. 239–244. First Joint International Conference on Recrystallization and Grain Growth, RWTH Aachen, Germany, August 27–31, 2001.

[14] Jones, H. The surface energy of solid metals. *Metal Sci. J. 5* (1971), 15–18.

[15] Kinderlehrer, D., Lee, J., Livshits, I., Rollett, A., and Ta'asan, S. Mesoscale simulation of the evolution of the grain boundary character distribution. *Mater. Sci. Forum 467–470* (2004), 1063–1068.

[16] Mackenzie, J. K. Second paper on statistics associated with the random disorientation of cubes. *Biom. 45*, 1 (1958), 229–240.

[17] Matsutani, S., Nakano, K., and Shinjo, K. Surface tension of multi-phase flow with multiple junctions governed by the variational principle. *Math Phys. Anal. Geom. 14* (2011), 237–278.

[18] Merriman, B., Bence, J. K., and Osher, S. J. Diffusion generated motion by mean curvature. In *Proceedings of the Computational Crystal Growers Workshop* (1992), J. Taylor, Ed., AMS, pp. 73–83.

[19] Merriman, B., Bence, J. K., and Osher, S. J. Motion of multiple junctions: a level set approach. *J. Comput. Phys. 112*, 2 (1994), 334–363.

[20] Mullins, W. W. Two-dimensional motion of idealized grain boundaries. *J. Appl. Phys. 27*, 6 (1956), 900–904.

[21] Patala, S., Mason, J. K., and Schuh, C. A. Improved representations of misorientation information for grain boundary science and engineering. *Prog. Mater. Sci. 57* (2012), 1383–1425.

[22] Read, W. T., and Shockley, W. Dislocation models of crystal grain boundaries. *Phys. Rev. 78*, 3 (1950), 275–289.

[23] Ruuth, S. J. A diffusion-generated approach to multiphase motion. *J. Comput. Phys. 145* (1998), 166–192.

[24] Sutton, A. P., and Balluffi, R. W. *Interfaces in crystalline materials*. Clarendon Press, Oxford, 2006.